Three-dimensional strain analysis using Mathematica

Matty Mookerjee [a],[*],[1], Scott Nickleach [b]

[a] Department of Geology, Sonoma State University, Rohnert Park, CA 94928, USA
[b] Department of Mathematics and Statistics, Sonoma State University, Rohnert Park, CA 94928, USA

ARTICLE INFO

ABSTRACT

A suite of geological computer programs written in Mathematica is currently available both within the online repository for the Journal of Structural Geology as well as on the first author's website (http://www.sonoma.edu/users/m/mookerje/ProgramPage.htm). The majority of these programs focus on three-dimensional strain analysis (e.g., determining best-fit strain ellipsoids, plotting elliptical data on either a Flinn or Hsu diagram, and determining error bounds for three-dimensional strain data). This program suite also includes a ternary diagram plotting program, a rose diagram program, an equal area and equal angle projections program, and an instructional program for creating two-dimensional strain path animations. The bulk of this paper focuses on a new method for determining a best-fit ellipsoid from arbitrarily oriented sectional ellipses and methods for determining appropriate error bounds for strain parameters and orientation data. This best-fit ellipsoid method utilizes a least-squares approach and minimizes the error associated with the two-dimensional data-ellipse matrix elements with the corresponding matrix elements from sectional ellipses through a general ellipsoid. Furthermore, a kernel density estimator is utilized to yield reliable error margins for the strain parameters, octahedral shear strain, Flinn's k-value, and Lode's ratio. By assuming a gamma distribution for the simulated principal axes orientations, more realistic error bounds can be estimated for these axes orientations.

© 2011 Elsevier Ltd. All rights reserved.

1. Introduction

Among its many applications, Mathematica is particularly useful for manipulating and graphically displaying data. While Mathematica is relatively user-friendly, building complex programs from scratch can be very time-consuming and is inefficient, considering that many Earth Science users are ultimately doing very similar types of analyses (for instance, see Haneberg's text, Computational Geosciences with Mathematica (Haneberg, 2004)). To this end, the first author has assembled a suite of seventeen Mathematica files that have applications for the earth sciences, with a particular emphasis on strain analysis (Table 1). This suite, as well as several sample data files, can be downloaded from the following website: http://www.sonoma.edu/users/m/mookerje/ProgramPage.htm.
Eight of the programs deal specifically with the process of determining a best-fit ellipsoid from sectional data sets. These programs utilize new methods for defining a best-fit ellipsoid, and four of them utilize a novel approach for determining the error bounds of the fit data in terms of both the ellipsoid shape and its orientation.

These methods are described in detail in Sections 3 and 4. The remaining nine programs are primarily graphical in nature.
For several decades, structural geologists have investigated three-dimensional strains and have illustrated how useful these techniques are for understanding the kinematics of deforming materials (e.g., Cloos, 1947; Flinn, 1962; Hossack, 1967; Gairola, 1977; Mitra, 1978; Wheeler, 1986; Dewey et al., 1998; Merschat et al., 2005; Galon et al., 2008; Mookerjee and Mitra, 2009; Thigpen et al., 2010). Additionally, many investigators have contributed to efforts for determining a best-fit ellipsoid from two-dimensional data. Initially, the methods were confined to three mutually perpendicular sections (Ramsay, 1967; Shimamoto and Ikeda, 1976; Oretel, 1978; Miller and Oertel, 1979), then three non-perpendicular section (Milton, 1980), and finally three or more non-perpendicular sections (Gendwill and Stauffer, 1981; Owens, 1984; Shao and Wang, 1984; Robin, 2002; Launeau and Robin, 2005). As with our proposed method, several investigators have employed some form of a least-squares approach (Oretel, 1978; Miller and Oertel, 1979; Shao and Wang, 1984). Robin (2002) provides an informative chronology for these contributions. Furthermore, Yonkee (2000) incorporated statistics into his best-fit ellipsoid program using a Monte Carlo simulation. Taking a similar, simulation-based approach, our method uses kernel density estimation to determine error bounds for the strain parameters,

* Corresponding author. Tel.: +1 707 664 2002; fax: +1 707 664 3975.
E-mail address: matty.mookerjee@sonoma.edu (M. Mookerjee).
[1] Formerly Matthew Strine.

Table 1
List of programs in the geological programs for Mathematica suite.

List of programs
Best-fit ellipsoid
Best-fit ellipsoid with statistics
Best-fit ellipsoid for ImageJ
Best-fit ellipsoid-absolute
Best-fit ellipsoid-absolute for ImageJ
Best-fit ellipsoid with statistics for ImageJ
Best-fit ellipsoid with statistics-absolute
Best-fit ellipsoid with statistics-absolute for ImageJ
Flinn plot
Flinn plot with error regions
Hsu plot
Hsu plot with error regions
Equal area & angle projections
Rose diagram
Ternary diagram
Section data through an ellipsoid
2D pure versus simple shear

octahedral shear strain (ε_s), Flinn's k-value, and Lode's ratio (ν). While this approach is new to the application of strain analysis, it is used for other applications in the earth sciences (e.g., grain size distributions (Buscombe, 2008), special distribution of volcanism (Connor et al., 2008), storm frequencies (Joyner and Rohli, 2010), mass extinctions (Wang, 2003), etc.). We believe that adding these sorts of confidence estimations to strain analysis will help investigators make informed and reasonable geological interpretations while providing feedback about their data collection techniques, and help them to decide when more data is needed to constrain a structural problem. The methods proposed in this contribution build on these investigators' work, and our program suite is intended to fulfill most of the computational and graphical needs of the structural geologist community for three-dimensional strain analysis.

2. Why Mathematica?

The primary reason for using Mathematica is that it allows for the relatively easy modification of the programs to suit the users' specific needs. While the programs are designed to accommodate many different user preferences, more specific user requirements will exist. Fortunately, Mathematica provides a favorable environment for user customization, including a very useful help system, on-line support forums, and their Technical Support Group. Mathematica runs on most operating systems (e.g., Windows, Mac OS, and Linux). Additionally, Wolfram Research ensures that new versions of Mathematica that are functional with older Mathematica files/programs. Finally, Mathematica has superb graphical capabilities which produce interactive three-dimensional plots (e.g., ellipsoids) and create animations, both of which usefully convey complex ideas and geometric relationships.

3. Determining the best-fit ellipsoid

The term "best-fit" is often employed with little thought for what criterion makes something the "best." With regards to a best-fit ellipsoid, our initial preference was to define the best fit as the one that has the minimum difference between the set of "mean" axial ratios (Rf) and "mean" angular orientations (ϕ) from the initial data set and those of a general ellipsoid (e.g., see the Methods section of Strine and Wojtal (2004)). This outcome is achieved by calculating the equations for the Rf and the ϕ of a specific plane in terms the matrix elements of a symmetric 3×3 matrix. These equations are then subtracted from their corresponding "mean" Rfs

and ϕs for the specific plane. Then, in a typical least-squares approach, the differences are squared and summed together, and this entire error function is minimized in terms of the six matrix elements. While this approach does yield reasonable results, we now believe that this method falls just short of generating the best fit because it treats the Rfs and the ϕs as independent parameters. If a two-dimensional strain marker is very nearly circular, its individual angular orientation is largely independent of the "mean" angular orientation. In contrast, the angular orientation of a strain marker with a relatively large aspect ratio should have a significantly greater effect on the "mean" angular orientation (e.g., Dunnet, 1969; Matthews et al., 1974; Shimamoto and Ikeda, 1976; Robin, 1977; Mulchrone et al., 2003; Choudhury and Mulchrone, 2006). Thus, simply using the vector and harmonic means as defined by Lisle (1985) neglects to account for this interdependence. A further weakness of the method proposed by Strine and Wojtal (2004) is that a quantitative judgment is required by the user on which parameter (Rf or ϕ) is weighted more heavily. This extra degree of freedom makes it difficult to call any solution the best fit.

Despite these imperfections in the Strine and Wojtal (2004) method, we appreciate the approach of minimizing the error between the input data and the fit solution. Furthermore, we suggest that any fitting method needs to be evaluated with this criterion in mind, i.e., a best-fit ellipsoid is the one that has the minimum difference between the input data and the fit solution. For this reason, the method that we propose involves the minimization of an error function, i.e., a function that represents that error associated with the difference between the input sectional data and any general ellipsoid. While this numerical approach may seem to employ brute force, particularly when compared to the more analytical solution of Robin (2002), we hope that our users will benefit from the transparency of our relatively simple procedure. We hope that demystifying this process will help investigators think more critically about the quality of their data and potentially make improvements and customizations to the software. During the testing of our method, we generated one hundred ellipsoids of random shape and orientation and calculated the sectional ellipses for three to six randomly oriented planes for each ellipsoid. This data set was used to compare the results of our program with those of Launeau and Robin (2005). The results were consistently similar in that the median angular difference between the two methods for the principal axes orientations is less than one degree, the median difference in octahedral shear strain was 0.004, and the median difference in Lode's ratio was 0.019. Therefore, we conclude that both methods are equally valid. We hope that users will find value in the customizability of our programs (e.g., adding a statistical analysis as described below) as well as the variety of graphical outputs.

3.1. Two-dimensional data

To begin fitting a three-dimensional ellipsoid to data, one first needs two-dimensional sectional data. Many methods exist for determining a two-dimensional "mean" ellipse (e.g., the Fry Method, Rf/ϕ, various Mohr circle methods, the Haughton–Breddin method of using fossils with bilateral symmetry, etc.). The resulting ellipses from any of these methods can be input into one of the best-fit ellipsoid programs (either manually or read in from a file). However, if an investigator has a data set of individual elliptical measurements (e.g., measurements from deformed quartz grains), then those data sets can be copied into the appropriate *.txt or *.xls file, and the program will read in this file and determine the "mean" elliptical shape for each of the sections automatically. The "mean"

ellipses are determined by averaging ellipse shape tensors as described by Shimamoto and Ikeda (1976) and Wheeler (1984).

The default sign convention for the best-fit ellipsoid programs is: 1) all sectional data are viewed looking downward, 2) perfectly vertical planes are viewed looking westward and if the vertical planes strike exactly east–west, the plane is viewed from the south to the north, 3) the orientation angle (ϕ) is measured from the long axis of the ellipse to the strike line of the sectional plane, 4) ϕ is positive when it has a positive slope and negative when it has a negative slope (Fig. 1a), and 5) for perfectly horizontal planes, ϕ is measured from the east–west line such that the NE quadrant is positive and the SE quadrant is negative. Because potential users may collect their data using the program ImageJ, an additional set of best-fit ellipsoid programs have been produced which are consistent with the sign convention employed by ImageJ (all programs with "for ImageJ" in the file name/title). For these programs, the sign convention number 4) differs. Instead of defining ϕ from $-90°$ to $+90°$, this program defines ϕ from 0 to 180°. Therefore, ϕ is always positive and is measured counterclockwise from the positive horizontal axis to the ellipse's principal long axis (Fig. 1b).

3.2. Assembling the error function

To assemble the error function, we first convert the initial data set into a set of 2×2 matrices. The mean axial ratio (Rf) for a given section can be inserted into a matrix in its principal reference frame:

$$PM = \begin{bmatrix} \sqrt{\dfrac{1}{Rf^2}} & 0 \\ 0 & \dfrac{1}{\sqrt{\dfrac{1}{Rf^2}}} \end{bmatrix}$$

(Ramberg, 1975; Tikoff and Fossen, 1993). This matrix can then be rotated into the appropriate orientation, i.e. by the angle ϕ, to yield the data matrix,
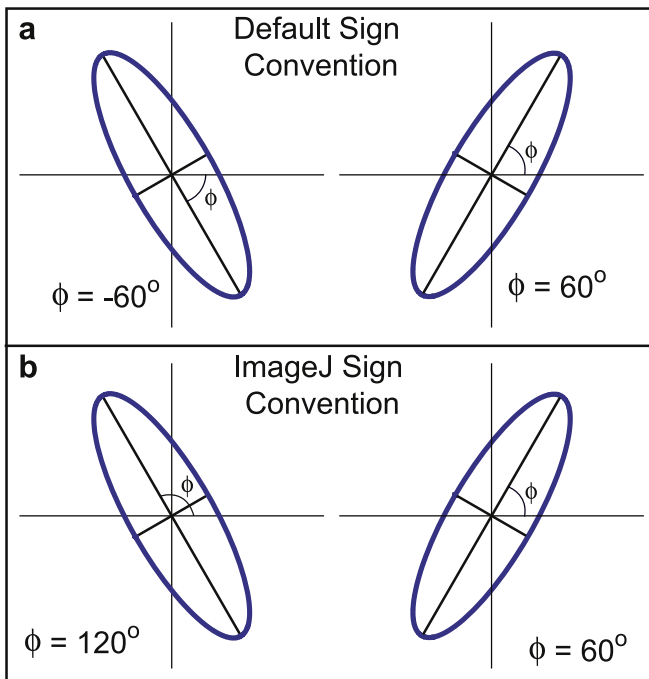

Fig. 1. a) Our default sign convention for the "Best-Fit Ellipsoid" programs, b) the sign convention used by ImageJ.

$$DM = \begin{bmatrix} Cos[\phi] & -Sin[\phi] \\ Sin[\phi] & Cos[\phi] \end{bmatrix} \cdot PM \cdot \begin{bmatrix} Cos[\phi] & Sin[\phi] \\ -Sin[\phi] & Cos[\phi] \end{bmatrix}$$

If the user wishes to determine the absolute size of the ellipsoidal marker, then she/he should use any of the best-fit ellipsoid programs with "absolute" in the file name/title. These programs do not use the axial ratio to assemble the PM matrix. Instead, they use the inverse of the squared lengths for the ellipse's principal axes for the diagonal elements of PM.

Next, we define what we call the general ellipsoid,

$$GE = \begin{bmatrix} \lambda_{xx} & \gamma_{xy} & \gamma_{xz} \\ \gamma_{xy} & \lambda_{yy} & \gamma_{yz} \\ \gamma_{xz} & \gamma_{yz} & \lambda_{zz} \end{bmatrix}$$

Any three-dimensional ellipsoid (or hyperboloid, as discussed below) can be represented in this form. We can then calculate the 2×2 matrix for the ellipse that results from cutting the general ellipsoid with a planar section through the center. This planar section is one of the planes from which the investigator has collected his/her data, and is input by the user in terms of the plane's dip and dip direction. To calculate the 2×2 matrix for the sectional ellipse, the general ellipsoid undergoes two independent rotations such that the planar section is parallel with one of the reference frame planes, where our reference frame is defined by north, east, and up (Fig. 2). This process is: 1) rotate the general ellipsoid such that the planar section is striking east–west (Fig. 2b),

$$VR = \begin{bmatrix} Cos[DipDir - 90°] & -Sin[DipDir - 90°] & 0 \\ Sin[DipDir - 90°] & Cos[DipDir - 90°] & 0 \\ 0 & 0 & 1 \end{bmatrix}$$
$$\cdot GE \cdot \begin{bmatrix} Cos[DipDir - 90°] & Sin[DipDir - 90°] & 0 \\ -Sin[DipDir - 90°] & Cos[DipDir - 90°] & 0 \\ 0 & 0 & 1 \end{bmatrix},$$

and 2) rotate the resulting matrix about the east–west line so that the planar section is vertical (Fig. 2c),

$$ER = \begin{bmatrix} 1 & 0 & 0 \\ 0 & Cos[90 - Dip] & -Sin[90 - Dip] \\ 0 & Sin[90 - Dip] & Cos[90 - Dip] \end{bmatrix}$$
$$\cdot VR \cdot \begin{bmatrix} 1 & 0 & 0 \\ 0 & Cos[90 - Dip] & Sin[90 - Dip] \\ 0 & -Sin[90 - Dip] & Cos[90 - Dip] \end{bmatrix}.$$

Now that the general ellipsoid is in the appropriate orientation, the corner elements of this matrix can be used to form a 2×2 matrix which represents the elliptical section through the general ellipsoid,

$$EM = \begin{bmatrix} ER_{11} & ER_{13} \\ ER_{31} & ER_{33} \end{bmatrix} \Big/ \left(\left(Det \begin{bmatrix} ER_{11} & ER_{13} \\ ER_{31} & ER_{33} \end{bmatrix} \right)^2 \right)^{\frac{1}{4}}$$

(Fig. 2d). Notice that the equation for EM includes dividing the matrix of the corner elements of ER by the square root of its determinate. This step ensures that the method works for axial ratios of approximately elliptical markers without requiring the absolute lengths of the axes, i.e. the EM matrix is normalized with respect to the ellipse area. The determinant is squared and then fourth-rooted instead of simply taking the square root to avoid the possibility of imaginary numbers. The best-fit ellipsoid programs that determine the absolute size of the ellipsoidal marker do not normalize the EM matrix.

At this point, the error associated with the data from a given plane with respect to the general ellipsoid can be calculated: $EF_i = (DM_{11,i} - EM_{11,i})^2 + (DM_{12,i} - EM_{12,i})^2 + (DM_{22,i} - EM_{22,i})^2$, where i is an indicator of the given data plane. By summing the
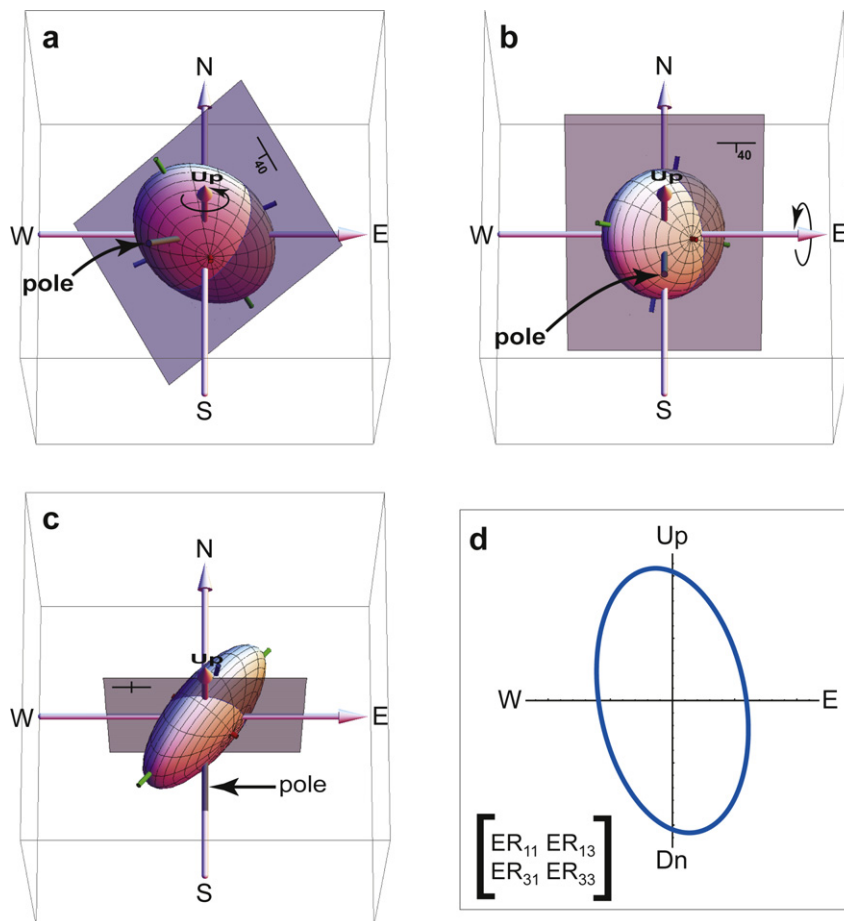
Fig. 2. a) While the illustrated ellipsoid is specified for graphical reasons, it represents all possible ellipsoids, i.e. the general ellipsoid, GE. The plane represents one of the planar sections from which an investigator has collected two-dimensional strain data, b) the general ellipsoid has been rotated such that the planar section is now striking E–W, c) the general ellipsoid has been further rotated so that the planar section is now vertical, d) this ellipse represents the elliptical section through the general ellipsoid for this specific plane along with the associated 2 × 2 matrix in terms of the general ellipsoid's matrix components.

error terms for each of the individual data planes, we obtain the overall error function:

$$\sum_{i=1}^{n}(DM_{11,i} - EM_{11,i})^2 + (DM_{12,i} - EM_{12,i})^2 + (DM_{22,i} - EM_{22,i})^2$$

where n is equal to the number of data planes ranging from a minimum of three to, theoretically, infinity. This function is now expressed in terms of the general ellipsoid and includes the entire strain data set (i.e., Rfs (or absolute ellipse principal axes lengths), ϕs, and the dips, and dip directions of data planes). For any given values of the λs and γs, the error function is a scalar quantity proportional to the "goodness" of the fit; the smaller this number, the better the fit. For the best-fit ellipsoid programs where the sectional data is in the form of axial ratios, determining the absolute size of the ellipsoid is not a goal. Thus, the error function can be further constrained by setting λ_{yy} equal to one. Now, all that remains is to minimize the error function. We do so with Mathematica's built-in "FindMinimum[]" function, which uses a minimization routine based on a steepest descent algorithm. In this way, we determine the best-fit ellipsoid.

Clearly, it is important also to report some measure of the compatibility of the initial two-dimensional data sets. We have chosen to report the mean of the absolute values of the differences between the initial data 2 × 2 matrix elements and those of the fit ellipsoid:

$$\frac{\sum_{i=1}^{n}\left(|DM_{11,i} - EM_{11,i}| + |DM_{12,i} - EM_{12,i}| + |DM_{22,i} - EM_{22,i}|\right)}{3 \times n}.$$

This "Mean Error," as we refer to it in the program output, effectively quantifies the difference between the initial input data set and the final fit solution.

As was mentioned above and by Launeau and Robin (2005), the class of matrices represented by GE also includes hyperboloids. A hyperboloid is defined by a symmetric 3 × 3 matrix with at least one negative eigenvalue. It is entirely possible that a hyperboloid fits a data set of ellipses better than an ellipsoid. To ensure against a hyperboloid solution, the best-fit ellipsoid programs constrain the FindMinimum[] function such that solutions with negative eigenvalues are not acceptable. However, this additional constraint does not alleviate the problem that the data set itself does not fully constrain the solution, i.e., more data are needed from an additional planar section. Thus, when the constraint in the FindMinimum[] function is necessary, it generally finds a solution which is near the boundary between the area defining hyperboloids and ellipsoids. All matrices in the class GE associated with this boundary have at least one eigenvalue equal to zero. Therefore, in these cases, the solution that the program will output is one for which an eigenvalue is nearly zero, which translates to a fitted ellipsoid with an unrealistically large long axis. While this is the best-fit ellipsoid for the given data set, the

program will output a suggestion to the user that she/he should most likely collect data from an additional planar section to further constrain the ellipsoid shape.

3.3. Graphical output

One of our goals for providing the best-fit ellipsoid programs is to provide users with an assessment of the quality of their data. Reporting the "Mean Error" is one important way of doing this. However, many users may lack an intuitive understanding for how this number relates to the compatibility of their initial data set. This issue is why having graphical representations of the sectional data is so important. Showing the users the initial input ellipse on top of the elliptical section through the fit ellipsoid for the same plane gives them an intuitive feel for the quality of their data (Fig. 3). In addition to the sectional ellipses, the best-fit ellipsoid programs output a representation of the ellipsoid in the geographic reference frame (both with representations of the sectional planes and without), a Flinn diagram (Flinn, 1962) with both Flinn's k-value and octahedral shear strain (ε_s) (Nadai, 1963) contrours, and a Hsu plot (Hossack, 1967) with both Lode's ratio (ν) and ε_s contours (Fig. 4a,b,d). For the best-fit ellipsoid programs that incorporate a statistical component, both the Flinn and Hsu plots include an error region (Fig. 4b,d). Additionally, the statistical programs include equal area projections of the set of principal axes orientations produced by the simulation (Fig. 4c). These graphical aids are intended to facilitate the investigator's ability to quickly evaluating his/her data as well as providing graphical elements for figures (e.g., Strine and Wojtal, 2004; Strine and Mitra, 2004).

4. Statistical analysis

Running the best-fit algorithm yields a best-fit ellipsoid for a given data set. However, this result does not give the user a sense of reliability for their initial data, as it conveys no information about the error margin associated with the fit. The user should not interpret a small "Mean Error" as an indication that the data have yielded an accurate solution. The "Mean Error" simply indicates that the input data are consistent with the fitted ellipsoid, but it is certainly possible for an ellipsoid to fit inaccurate data very well.

4.1. Non-applicability of standard large-sample theory

One common approach for obtaining error bounds is to rely on the Central Limit Theorem and utilize the Multivariate Delta Method. Two factors prohibit us from pursuing such a route to construct the error bounds for our parameters of interest. First, the function used to determine the best-fit ellipsoid is complicated. Consequently, calculating the partial derivatives required to utilize the Multivariate Delta Method is cumbersome. The second factor, the incorporation of measurement error in the orientations of the data planes, is even more problematic. The fact that the perceived planar orientations can differ from true orientations has a very similar effect to measurement error in the actual elliptical data. Working in the presence of measurement error can cause the standard large-sample theory to break down. The means and/or variances of the approximating normal distributions are generally not the same as the true theoretical quantities. Given this, we pursue an alternative approach.

4.2. A simulation-based approach to obtaining error bounds

Being unable to use the standard theoretical machinery, we apply an iterative simulation-based approach similar to Yonkee (2000) to gain insight into the error margins associated with fitted ellipsoids and any parameters estimated from that fit. This approach helps determine how sensitive the fitted ellipsoid is to small changes in the input data. Ostensibly, if small changes in the input data result in small changes in the fit, then one can perceive the fit to the initial data set as relatively reliable. Conversely, if small changes in the data lead to vast changes in the fit, then clearly one must interpret the original best-fit solution with caution.

The simulation consists of several steps. The first step is to calculate the mean values of Rf and ϕ for each of the cross-sectional samples, as described above. These values, along with the orientations of the planar sections are used to obtain the best-fit ellipsoid. Next, the iterative procedure begins by randomly perturbing each pair (Rf and ϕ) of mean values. The values of these perturbations are obtained by randomly drawing an observation from a bivariate normal distribution with a mean vector equal to zero and a variance covariance matrix obtained from the corresponding elliptical data sets. In so doing, we essentially estimate the sample
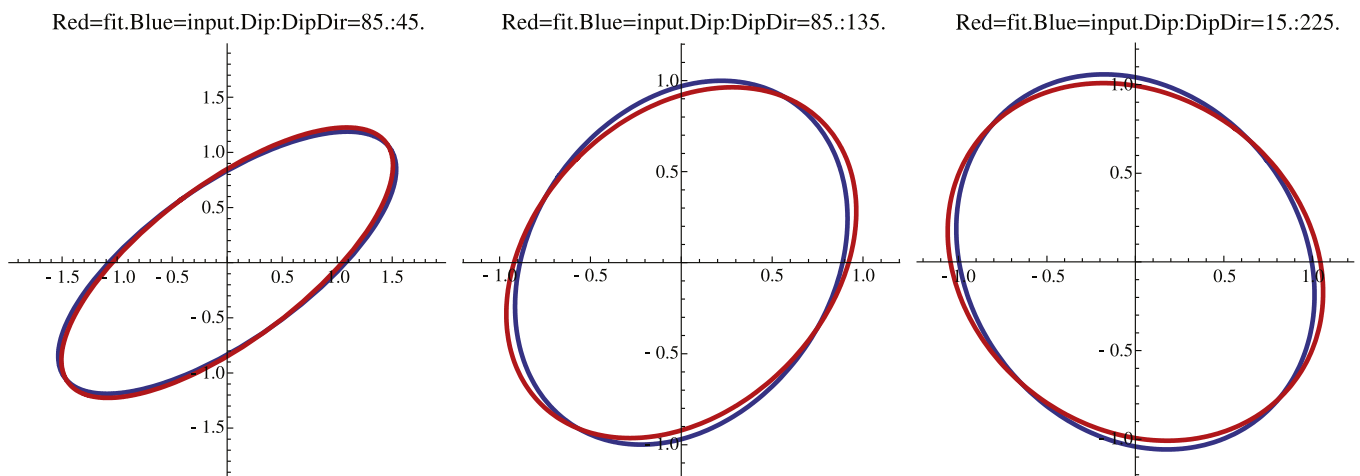

Fig. 3. Section ellipses output from the "Best-Fit Ellipsoid" program. The red ellipse is the initial input data and the blue ellipse is the elliptical section through the fit ellipsoid for a given planar orientation. (For interpretation of the references to color in this figure legend, the reader is referred to the web version of this article.)
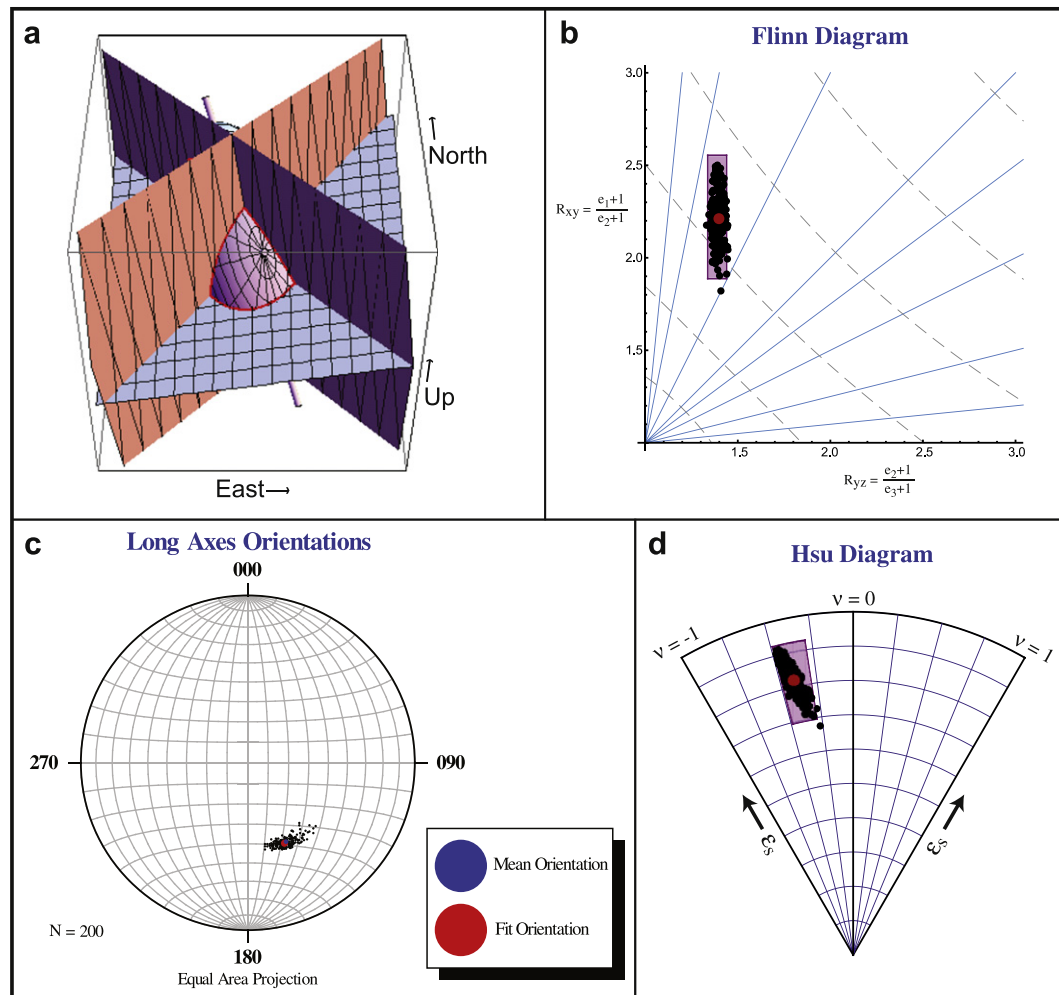
Fig. 4. Graphical output of the "Best-Fit Ellipsoid with Statistics" program. a) best-fit ellipsoid with the sectional planes represented cutting through the center of the ellipsoid, b) Flinn diagram with the best fit and simulation-derived data and the resulting error region, c) equal area plot of 200 ellipsoid long axes produced during the simulation, and d) Hsu plot with the best fit and simulation-derived data and the resulting error region.

distribution for each pair of elliptical data (Rf and ϕ) with a specific correlation calculated from the initial data set, and then randomly generating a value from these bivariate normal distributions. Furthermore, the orientations of the collection planes for the elliptical data are also randomly perturbed, each by a value randomly generated from a normal distribution with a mean equal to zero and a standard deviation specified by the user. A best-fit ellipsoid is then fit to this collection of new input values. Finally, this procedure can be repeated indefinitely so as to obtain a population of best-fit ellipsoids from which a statistical analysis can be performed.

The first type of random perturbation helps the user to understand the effect that natural variation in the estimates of the true mean values of the Rf's and ϕ's might have on the fitted ellipsoid. The perturbation of the sectional plane orientations helps to quantify the effect of measurement error on the best-fit solution. By conducting a large enough number of iterations and examining the collection of fitted ellipsoids, one gains a notion of the error magnitude associated with the best-fit ellipsoid. Our way of examining this collection of ellipsoids is to uses a technique known as kernel density estimation. This technique determines the error bounds for the ellipsoid shape parameters, i.e., octahedral shear strain (ε_s), Lode's ratio (ν) and Flinn's k-value. Since the ellipsoid

size is not a contributing factor to the values of these parameters, the axes lengths are normalized such that the intermediate axis has unit length. Consequently, these ellipsoidal shape parameters are functions of two values, namely the lengths of the long (λ_1) and short (λ_3) axes. Point estimates of each parameter value are thus obtained by applying the appropriate functions to the values of the λ_1 and λ_3 of the best-fit ellipsoid. To provide error margins along with the point estimates, we fit a kernel density estimator to the collection of values of λ_1 and λ_3 of the ellipsoids generated in this iterative.

Kernel density estimation is a non-parametric method of estimating the probability density function of a random variable or random vector. The kernel density estimator (KDE) is constructed by placing a kernel function at each of a collection of values. A handful of kernel functions are commonly used. Of those, we used a bivariate normal kernel function. Additionally, when fitting a two-dimensional KDE, one must specify two bandwidths, which we set for the λ_1 direction and the λ_3 direction. Although these bandwidth parameters can heavily influence the shape of the density estimator, especially its peakedness, we will primarily be interested in calculating volumes under the KDE. As volume calculations tend to not be significantly sensitive to peakedness, it is adequate to use the fairly standard bandwidths:

$$h_i = 4 \times 1.06 \times \min\{\sqrt{\mathrm{Var}(L_i)}, \mathrm{IQR}_i/1.34\} \times N^{-1/5},$$

for $i = 1, 3$

where L_1 and L_3 represent the collection of long and short axis measurements obtained from the iterative process, IQR_1 and IQR_3 are the interquartile ranges of L_1 and L_3, and N is the number of iterations. Wasserman (2004) and Hastie et al. (2001) provide excellent introductory expositions about kernel density estimation.

The value of the KDE at any given point is the average of all of the individual kernel values:

$$\mathrm{KDE}[\lambda_1, \lambda_3] = \frac{1}{2\pi \times N \times h_1 \times h_3} * \sum_{i=1}^{N} \exp\left[-\frac{1}{2}\left(\left(\frac{\lambda_1 - L_{1,i}}{h_1}\right)^2 + \left(\frac{\lambda_3 - L_{3,i}}{h_3}\right)^2 \right) \right]$$

This results in the KDE having large values for regions which contain many points, and small values for regions containing few or no points. After calculating the KDE, one can interpret its value as a relative likelihood. The random quantity that the KDE is modeling is more likely to assume a value where the KDE is large than where it is small. Fig. 5a illustrates an example of a KDE generated from the "Best-Fit Ellipsoid with Statistics" program.

Once the KDE for λ_1 and λ_3 is constructed, we use it to obtain error bounds for the point estimates of the various parameters. The first step is to specify a desired degree of certainty associated with the error margin (95% is the default value). Next we determine the smallest region in λ_1 versus λ_3 space such that the volume of the space above this region to the KDE is approximately 0.95. To do so, consider a set in the $\lambda_1 - \lambda_3$ plane such that the integral of the KDE over the set is at least 0.95. Now, let $\mathscr{A}$ represent the class of all such sets, define $A_z = \{(\lambda_1, \lambda_3) : \mathrm{KDE}(\lambda_1, \lambda_3) > z\}$, and let $I(z)$ be the integral of the KDE over A_z. Note that for $0 \leq z \leq \mathrm{KDE}_{\max}$, I is a decreasing function of z and ranges from 1 to 0 as z ranges from 0 to $\mathrm{KDE}_{\max}$, respectively. Consequently, it has an inverse function with domain $[0,1]$, say $I^{-1}(v) = z$. Let $I^{-1}(0.95) = z'$. Then A_z is in $\mathscr{A}$, and no other set in $\mathscr{A}$ has an area smaller than $A_{z'}$. Computationally, we obtain the set $A_{z'}$ as an approximating set of rectangles (Fig. 5b). The user can specify a value (0.0001 by default) to control the magnitude of the error associated with this approximation.

To obtain error margins for ε_s, v, and k, we calculate their values at the center of each rectangle contained in the collection used as the approximation of $A_{z'}$. Each of the resulting ranges of values is taken as the interval estimate for the corresponding parameter. Our experience suggests that this method tends to be fairly conservative. By this, we mean that if we interpret the ranges as confidence intervals for the unknown parameters, then our true level of confidence that the range contains the theoretical value of the parameter is somewhat larger than the input degree of uncertainty (e.g., 95%). While this situation may not be ideal as it gives rise to larger interval estimates, we find this situation more acceptable than the converse. Fig. 6 illustrates an example of a strain analysis conducted on five samples taken from the Bitterroots Detachment Lobe, Montana. Notice that two samples have very large error bounds in terms of their Flinn's k-value (Fig. 6d). Understanding the relative reliability of each of these strain data points will assist in making the most reasonable kinematic interpretations of the data set.

4.3. Error bounds for axes orientation

In addition to determining error margins for the ellipsoid shape parameters, the statistical programs also provide error bounds for the orientation of the ellipsoid principal axes. While observing the distribution of the simulation-derived axes orientations with respect to their angle away from the best-fit axis, we found that the orientations appeared to follow a gamma distribution (Fig. 7). After fitting a gamma density to the orientations, this density function can be used in much the same way the kernel density estimate was used to find error bounds. More specifically, we can simply integrate the fitted gamma density to find the smallest range containing 95% of the distribution. In doing so, we provide a margin of error associated with our point estimate of axis orientation. While some investigators may be more comfortable using Fisherian statistics and calculating an "alpha" angle, as is often used during paleomagnetic studies in which α_{95} is a fairly standard parameter (e.g., Butler, 1992), we propose that the gamma distribution-derived error margin is more easily interpreted and likely more accurate. The α_{95} angle is generally an order of magnitude less than the gamma angle for simulations where N equals one hundred. It is known in
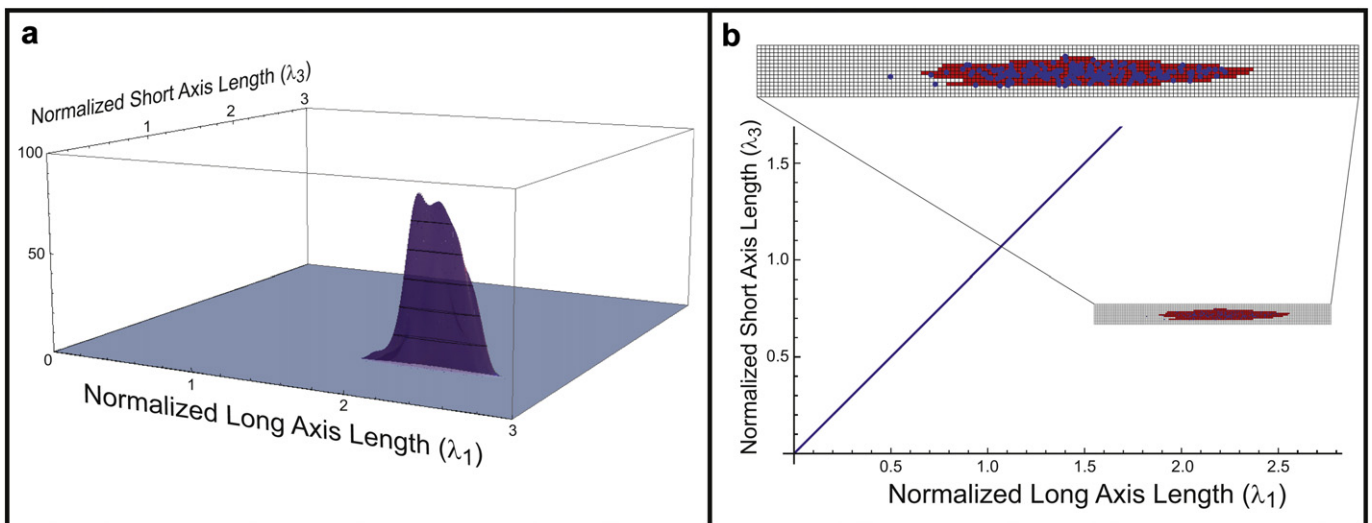

Fig. 5. a) The kernel density estimation surface generated from a simulation-derived data set from the "Best-Fit Ellipsoid with Statistics" program, b) the two-dimensional rectangular grid underneath the kernel density estimation delimiting the 95% error boundary.
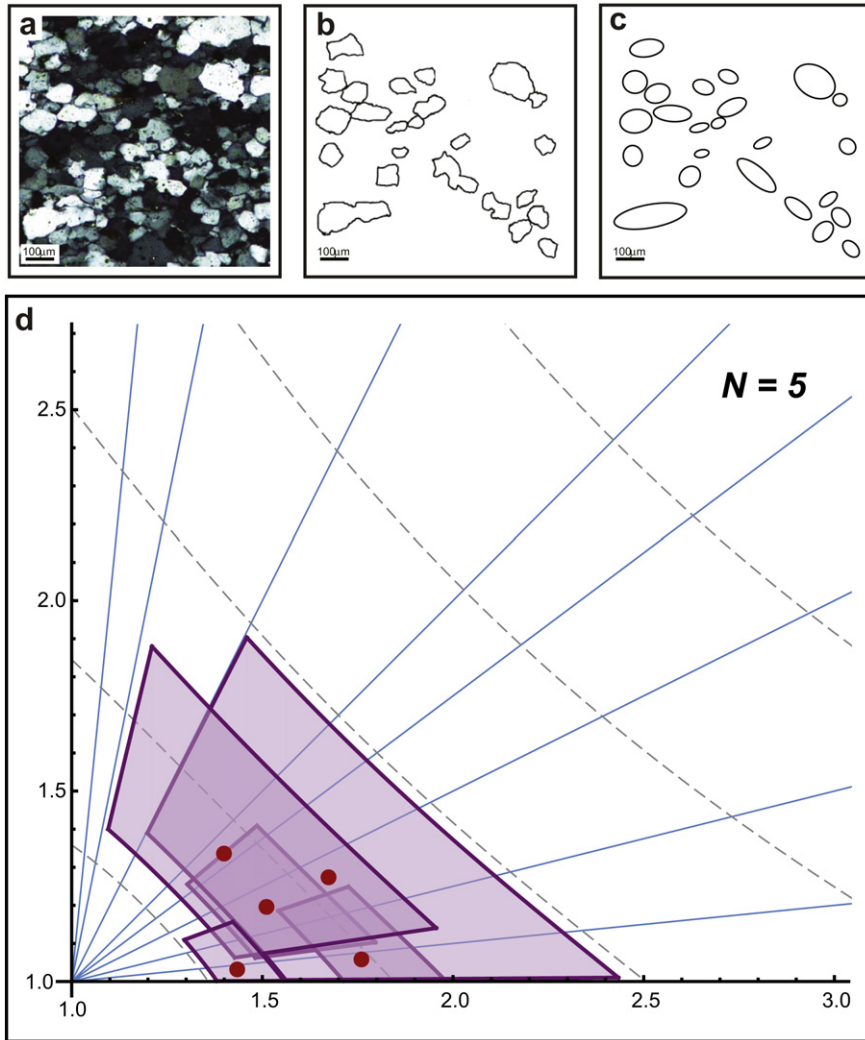
Fig. 6. Three-dimensional strain analysis from five samples collected from the Bitterroots Detachment Lobe, Montana. a) typical photomicrograph from the detachment zone, b) digital quartz grain tracings created using a tablet monitor, c) best-fit elliptical grain shape approximations determined using ImageJ, d) Flinn diagram output from the program "Flinn Plot with Error Regions." Octahedral shear strain contour interval is 0.25 and k-value contours = 10, 5, 2, 1, 0.75, 0.5, 0.25, and 0.1. These contour values are visible in Mathematica when the user mouses over any of the lines.

paleomagnetics that over-sampling can unrealistically reduce the α_{95} angle (Butler, 1992). Therefore, for strain analysis where the simulation can have as many iterations as the user wishes, we suggest that the gamma distribution-derived values be used. Still,

the statistical best-fit ellipsoidal program can calculate an α angle; although, by default, this feature is turned off.

The user may discover that their gamma distribution-derived error angle is particularly large because two of the three principal
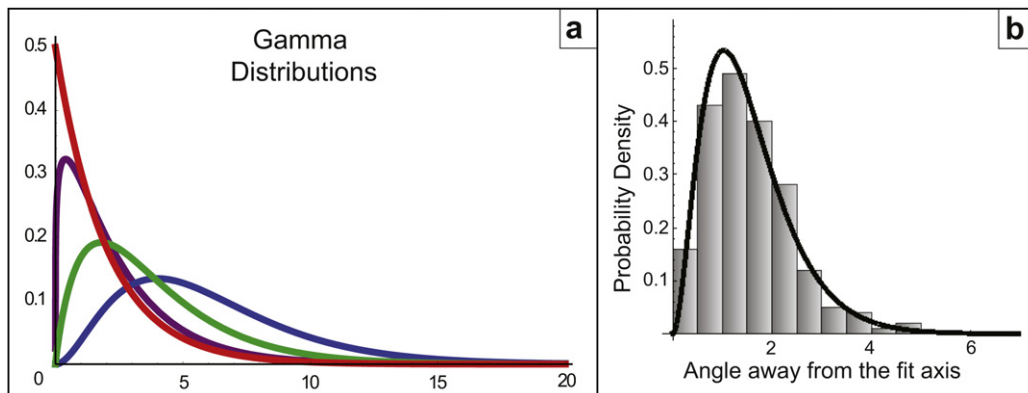

Fig. 7. a) Example of gamma distributions. Note that exponential decay is a special case of a gamma distribution, b) histogram of the angle between the simulation-derived axes orientations with respect to the best-fit axis with the corresponding gamma function overlain.

axes are very similar in lengths (i.e., nearly prolate or nearly oblate ellipsoids) and small variations in the data will drastically change their orientation. However, this variation is not random about a mean orientation, but instead defines a plane. In this case, reporting the large error angle does not tell the full story. For this reason, when the program detects this case, it also fits a plane to the axes orientations, and reports the orientation of that plane and the mean difference angle between the axes and the best-fit plane. This phenomenon can be observed by running the sample file "Sample Strain Data with Std Dev-ABS.xls" in the "Best Fit Ellipsoid with Statistics-Absolute" program. The statistical best-fit ellipsoid programs attempt to fit a plane to axes orientation data if the error angle is above a prescribed amount (the default is set at $5°$) and will report the orientation of that best-fit plane only if the mean difference angle is small enough (the default is set at $1°$).

5. Discussion

5.1. Strain analysis

We present a suite of strain analysis programs designed to provide transparency with respect to the quality of the user-provided data set. During its development, the Best-Fit Ellipsoid program was extensively tested with many different ellipsoid shapes and orientations, number of data planes, and data plane orientations (over 3000 combinations in total). Testing showed that certain combinations of planes and ellipsoid orientations are more prone to yielding a hyperbolic solution. When varying the length of the long axis of the ellipsoid changes the sectional ellipses only marginally, hyperbolic solutions are not uncommon. For instance, imagine four planes all dipping $45°$ and with evenly distributed dip directions. Now imagine these planes cutting through the center of a prolate ellipsoid with a vertical long axis. Changing the length of this long axis from 10 to 20 (while the other two axes are set at one) does not significantly alter the aspect ratio of the resulting elliptical section (only by ≈ 0.005) and does not change the angular orientations at all. Strain analysis of this example could easily lead to a hyperbolic solution. Moreover, the octahedral shear strains for these two ellipsoids are considerably different. Even if the data did not result in a hyperbolic solution, performing a statistical analysis is necessary to illustrate the data's sensitivity to small perturbations by yielding very large error estimate with respect to the ε_s. In this example, the investigator should collect additional data from a section that approximately contains the long axis of the ellipsoid to further constrain the solution.

Ultimately, we feel that investigators will be advantaged by being more thoughtful when choosing the orientations of their data planes. Given that always using three mutually perpendicular sections does not always yield the best results, investigators need a way to evaluate the effect of their sectional plane choices on the final result. One problem with using three mutually perpendicular sections is that investigators often choose the foliation plane as one of the planes, which, for many deformed rocks, is the worst plane for collecting data because the foliation plane is often defined by mineralogical and textural variation rather than strain geometry. While the first author admits to using this plane for collecting strain data in the past, with further consideration, it seems ill-advised to choose a plane that by its very nature can yield vastly different results depending on which foliation surface one happens to observe. We recommend that investigators performing a strain analysis, whenever possible, utilize a more iterative approach. While three data planes may be an appropriate number of planes to start a strain analysis, we suggest that after completing a statistical analysis an investigator should evaluate whether a strategically placed additional section would significantly further constrain the solution.

In addition to the standard kinematic parameters, the best-fit ellipsoid program presents the option of calculating a new kinematic parameter. At the very bottom of the code, the user can evaluate the last cell and calculate the out-of-plane natural strain (ε_{OP}). To be able to calculate this parameter, the user needs to know the orientation of the regional motion plane/shear plane. The program will then calculate the natural strain ($Ln[l/l_0]$) in the direction perpendicular to this plane. While the program automatically plots the data on both Flinn and Hsu plots, these plots neglect to account for the orientation of the strain ellipsoid. For instance, a plane strain ellipsoid (i.e., where $k = 1$ and $v = 0$) oriented with its long axis perpendicular to the thrusting direction does not represent a plane strain deformation. ε_{OP} will specify how much material is moving laterally, which in this case would be significant despite being a "plane strain" ellipsoid. This calculation (as with all of the strain parameters) assumes no volume loss.

6. Conclusions

The "Geological Programs for Mathematica" is a suite of programs for geologists to undertake quantitative analysis with a particular focus on strain analysis. The authors hope that these programs will facilitate the undertaking of three-dimensional strain analysis by more investigators, leading to more thoughtful selection of sectional data planes and reporting error bounds along with kinematic data.

Acknowledgments

Appendix. Supplementary material

Supplementary data associated with this article can be found, in the on-line version, at doi:10.1016/j.jsg.2011.08.003.

References

Buscombe, D., 2008. Estimation of grain-size distributions and associated parameters from digital images of sediment. Sedimentary Geology 210, 1–10.

Butler, R.F., 1992. Paleomagnetism: Magnetic Domains to Geologic Terranes. Blackwell Sci. Publ., Boston, 319 pp.

Choudhury, K.R., Mulchrone, K., 2006. A comparative error analysis of manual versus automated methods of data acquisition for algebraic strain estimation. Tectonophysics 421, 209–230.

Cloos, E., 1947. Oolite deformation in the South Mountain fold, Maryland. Geological Society of America Bulletin 58, 843–918.

Connor, C.B., Conner, L.J., Wetmore, P.H., 2008. Estimating the spatial intensity of volcanism. Geological Society of America: Abstracts with Programs 40 (6), 114.

Dewey, J.F., Holdsworth, R.E., Strachan, R.A., 1998. Transpression and transtension zones. In: Geological Society Special Publications, vol. 135 1–14.

Dunnet, D., 1969. A technique of finite strain analysis using elliptical particles. Tectonophysics 7, 117–136.

Flinn, D., 1962. On folding during three-dimensional progressive deformation. Quarterly Journal of the Geological Society of London 118, 385–433.

Gairola, V.K., 1977. Three-dimensional strains in fold-hinge zones. Tectonophysics 41, 291–319.

Galon, M.A., Kerns, S., Burmeister, K.C., 2008. STRAIN3D: a new computer program for graphical and statistical 3D strain analysis. Geological Society of America: Abstracts with Programs 40 (1), 65.

Gendwill, D.J., Stauffer, M.R., 1981. Analysis of triaxial ellipsoids: their shapes, plane sections, and plane projections. Mathematical Geology 13, 135–152.

Haneberg, W.C., 2004. Computational Geosciences with Mathematica. Springer-Verlag, Heidelberg, 381 pp.

Hastie, T., Tibshirani, R., Freidman, J., 2001. The Elements of Statistical Learning: Data Mining, Inference, and Prediction. Springer-Verlag, New York, 768 pp.

Hossack, J.R., 1967. Pebble deformation and thrusting in the Bygdin Area (southern Norway). Tectonophysics 5, 315–339.

Joyner, T.A., Rohli, R.V., 2010. Kernel density estimation of tropical cyclone frequencies in the Northern Atlantic Basin. International Journal of Geosciences 1, 121–129.

Launeau, P., Robin, P.-Y.F., 2005. Determination of fabric and strain ellipsoids from measured sectional ellipses—implementation and applications. Journal of Structural Geology 27, 2223–2233.

Lisle, R., 1985. Geological Strain Analysis; A Manual for the R_f/ϕ Technique. Pergamon Press, Oxford, 99 pp.

Matthews, P.E., Bond, R.A.B., Van Den Berg, J.J., 1974. An algebraic method of strain analysis using elliptical markers. Tectonophysics 24, 31–67.

Merschat, A.J., Hatcher, R.D., Davis, T.L., 2005. The northern Inner Piedmont, southern Appalachans, USA: kinematics of transpression and SW-directed mid-crustal flow. Journal of Structural Geology 27, 1252–1281.

Miller, D.M., Oertel, G., 1979. Strain determination from the measurement of pebble shapes: a modification. Tectonophysics 55, T11–T13.

Milton, N.J., 1980. Determination of the strain ellipsoid from measurement on any three sections. Tectonophysics 64, T19–T27.

Mitra, S., 1978. Microscopic deformation mechanisms and flow laws in quartzites within the South Mountain Anticline. Journal of Geology 86, 129–152.

Mookerjee, M., Mitra, G., 2009. Understanding kinematic data from the Moine thrust zone in terms of a kinematic-based mathematical model of deforming thrust wedges. Journal of Structural Geology 31, 1556–1572.

Mulchrone, K.F., Sullivan, F.O., Meere, P.A., 2003. Finite strain estimation using the mean radial length of elliptical objects with bootstrap confidence intervals. Journal of Structural Geology 25, 529–539.

Nadai, A., 1963. Theory of Flow and Fracture of Solids – Engineering Societies Monographs. McGraw-Hill, New York, 705 pp.

Oretel, G., 1978. Strain determination from the measurement of pebble shapes. Tectonophysics 50, T1–T7.

Owens, W.H., 1984. The calculation of a best-fit ellipsoid from elliptical sections on arbitrarily orientated planes. Journal of Structural Geology 6, 571–578.

Ramberg, H., 1975. Particle paths, displacement and progressive strain applicable to rocks. Tectonophysics 28, 1–37.

Ramsay, J.G., 1967. Folding and Fracturing of Rocks. McGraw-Hill, New York, 586 pp.

Robin, P.-Y.R., 1977. Determination of geologic strain using randomly oriented strain markers of any shape. Tectonophysics 42, T7–T16.

Robin, P.-Y.F., 2002. Determination of fabric and strain ellipsoids from measured sectional ellipses—theory. Journal of Structural Geology 24, 531–544.

Shao, J., Wang, C., 1984. Determination of strain ellipsoid according to two-dimensional data on three or more intersecting planes. Mathematical Geology 16, 823–833.

Shimamoto, T., Ikeda, Y., 1976. A simple algebraic method for strain estimation from deformed ellipsoidal objects—I. Basic theory. Tectonophysics 36, 315–337.

Strine, M., Mitra, G., 2004. Preliminary kinematic data from a salient-recess pair along the Moine thrust, NW Scotland. In: Sussman, A., Weil, A. (Eds.), Geological Society of America Special Paper, vol. 383, pp. 87–107.

Strine, M., Wojtal, S.F., 2004. Evidence for non-plane strain flattening along the Moine thrust, Loch Srath nan Aisinnin, North-West Scotland. Journal of Structural Geology 26, 1755–1772.

Thigpen, J.R., Law, R.D., Lloyd, G.E., Brown, S.J., 2010. Deformation temperatures, vorticity of flow, and strain in the Moine thrust zone and Moine nappe: reassessing the tectonic evolution of the Scandian forelandehinterland transition zone. Journal of Structural Geology 32, 9920–9940.

Tikoff, B., Fossen, H., 1993. Simultaneous pure and simple shear: the unifying deformation matrix. Tectonophyiscs 217, 267–283.

Wang, S.C., 2003. On the continuity of background and mass extinction. Paleobiology 29, 455–467.

Wasserman, L., 2004. All of Statistics: A Concise Course in Statistical Inference. Springer, New York.

Wheeler, J., 1984. A new plot to display the strain of elliptical markers. Journal of Structural Geology 6, 417–423.

Wheeler, J., 1986. Average properties of ellipsoidal fabrics: implications for two- and three-dimensional methods of strain analysis. Tectonophyics 126, 259–270.

Yonkee, A.W., 2000. Strain analysis incorporating bootstrap statistics and Monty Carlo simulations. Geological Society of America: Abstracts with Programs 32 (7), 227.